Discrete rearranging disordered patterns, part II: 2D plasticity, elasticity and flow of a foam

Philippe Marmottant, Christophe Raufaste, François Graner

EPJ manuscript No.
(will be inserted by the editor)

Plastic deformation in a flowing foam: measurement and prediction

P. Marmottant [a], C. Raufaste, and F. Graner

Laboratoire de Spectrométrie Physique, UMR5588, CNRS-Université Grenoble I, B.P. 87, F-38402 St Martin d'Hères Cedex, France

December 21, 2007

Abstract. The plastic flow of a foam results from bubble rearrangements. We study their occurrence in experiments where a foam is forced to flow in 2D: around an obstacle, through a narrow hole, or sheared between rotating disks. We describe their orientation and frequency using a topological tensor which links them with macroscopic plasticity. We then suggest a phenomenological equation to predict the plastic strain rate: its orientation is determined from the foam's local elastic deformation and its rate is determined from the foam's local elongation rate. We obtain a good agreement with statistical measurements. This helps describing the foam as a continuous medium with fluid, elastic and plastic properties, which is the goal of the companion paper [1].

PACS. 83.80.Iz Emulsions and foams – 83.10.Bb Kinematics of deformation and flow – 62.20 Deformation and plasticity

1 Introduction

A liquid foam, made of gas bubbles surrounded by liquid walls (Fig. 1), is elastic for small deformation, plastic for large deformation, and flows at large deformation rates [2,3]. The companion paper [1] provides definitions, notations and tools to explore this complex behaviour, but leaves largely open the question of transition from elastic to plastic regime. The present paper, which is *not self-contained*, presents an equation to describe this transition, tests its predictions on experiments on different foams, shows that it closes the system of equations describing a foam, and discusses possible applications to other systems.

A crucial step would consist in predicting the occurrence and properties of the individual plastic events [9], which in foams are the topological rearrangements (neighbour swapping, also called "T1 processes" [2]. Such a bubble rearrangement is instantaneous and implies a change from a stable elastic branch to another. It is followed by a relaxation leading to an *irreversible* and therefore plastic change in deformation and stress (Fig. 2). On the other hand, bubble rearrangements are the only source of irreversibility. Foams are unique material in the sense that a T1 process is equivalent to a plastic deformation. The relaxation time $\tau_{\rm relax}$ following a T1 in foams is determined by the dissipation; the rate of T1s is determined by the shear rate, which we keep slower than $\tau_{\rm relax}^{-1}$ in what follows (for extension to higher shear rates, see [10]). Ordered foams, where bubbles are arranged in a honeycomb lattice, are models for the plasticity of crystals based on dislocation movement [11,12,13]. Disordered foams, which we consider here, are models for the plasticity of amorphous materials: topological rearrangements are less correlated; when averaged over time or space their effect is usually smooth, and the foam behaves as a continous material (Fig. 3).

In the present article we tackle the following questions: Does one necessarily require a detailed microscopic understanding of velocity fluctuations and T1 correlations [16]? Else, is a continuous description based on coarse-grained quantities sufficient? For instance, recent quasistatic simulations relate the T1s' orientations with the local stress [17].

The continuous description considers coarse grained deformations of the material. The total applied deformation rate (or velocity gradient) contributes in part to load the elastic strain (bubbles deform) and to the plastic deformation rate (bubbles move relatively to each other). We want to write a kinematic equation for plasticity, which describes how the total deformation rate is shared between change of elastic strain and plastic deformation rate. In the scalar case the total applied deformation rate is the sum of the internal elastic strain rate and the irreversible plastic deformation rate:

$$\dot{\varepsilon} = \frac{d\varepsilon_{el}}{dt} + \dot{\varepsilon}_{pl}, \tag{1}$$

where we used a different notation for the time derivative of ε_{el}, to stress that it is a state variable. A kinematic equation for the plastic rate of slowly sheared foams is

[a] Author for correspondence at philippe.marmottant@ujf-grenoble.fr

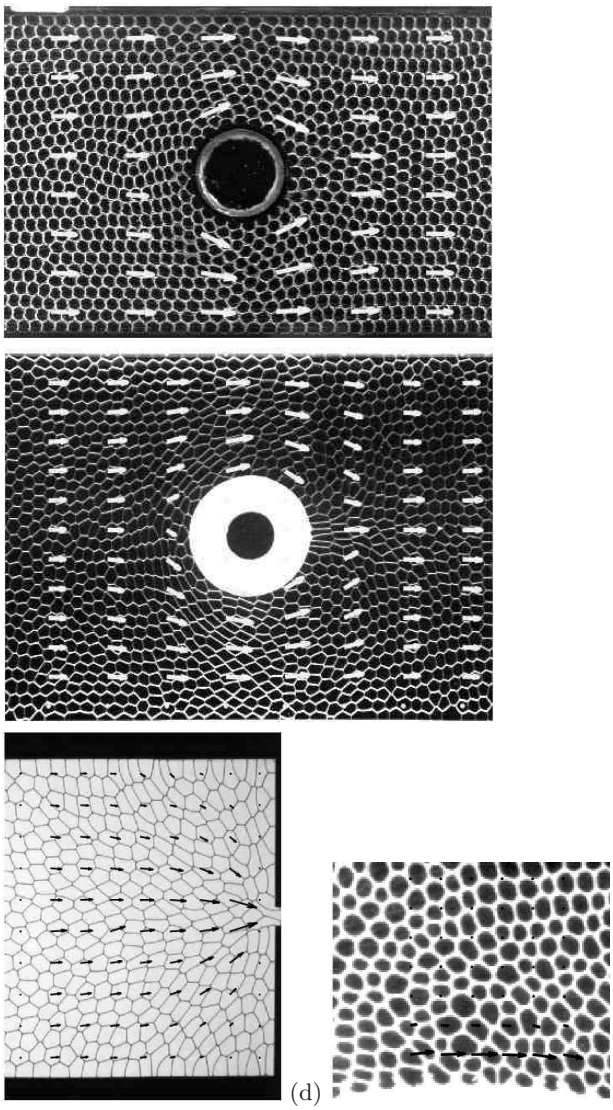

Fig. 1. Experimental 2D flows of a foam : top view, here flow from left to right. Field of view 15 cm × 10 cm. (a) Wet foam (between glass and water) flowing around an obstacle, picture B. Dollet [4]. (b) Dry foam (between parallel glass plates) flowing around an obstacle, picture C. Raufaste. [1]. (c) Moderately dry foam (between parallel plexiglass plates) flowing through a narrow hole, picture M. Asipauskas [5] (d) Wet foam (between parallel glass plates) sheared between two concentric wheels with tooth-shaped boundaries to prevent slipping; the rotating inner wheel is visible at the bottom, the fixed outer wheel is visible at the top; arrows indicate the measured velocity field [6]. Liquid fractions are only approximately estimated: (a) 4 10^{-2} [7], (b) 10^{-4} [8], (c) 10^{-2} [5], (d) 5 10^{-2} [6].

[15]:

$$\dot{\varepsilon_{pl}} = h(\varepsilon_{el})\dot{\varepsilon}, \tag{2}$$

if ε_{el} and $\dot{\varepsilon}$ have the same sign (loading of the material), and is zero if they have opposite signs (unloading). The plasticity fraction, or *yield function*, h, involves at least one material dependent parameter, the yield strain: h is zero at zero deformation, and reaches 1 at the yield strain. Eq. (2) closes the system of kinematic equations describing

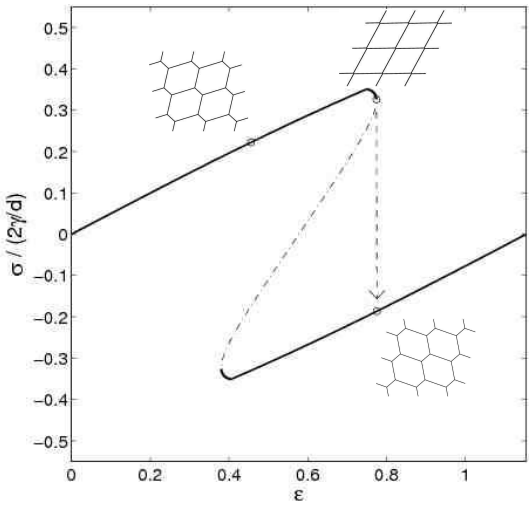

Fig. 2. Shear of a 2D ordered foam [14] (here with a fluid fraction 99%): the topological rearrangement occurs when the stress versus strain curve becomes unstable (dotted line) and induces an irreversible deformation. Three foams state are represented (circles on curve). The stress σ is here normalised using surface tension γ and bubble radius d.

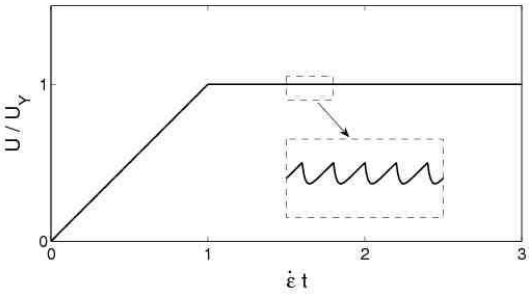

Fig. 3. Schematic impact of individual microscopic rearrangements on the stored elastic strain U, for a constant loading rate $\dot{\varepsilon}$. Rearrangements relax exponentially the strain over a time τ_{relax}, with here $\dot{\varepsilon}\tau_{\text{relax}} = 0.02 \ll 1$. In the present macroscopic model, rearrangements are coarse-grained. Reprinted from ref. [15].

a foam. Indeed from equation (1) and (2), we can integrate the internal elastic strain from a given applied deformation rate with $d\varepsilon_{el}/dt = \dot{\varepsilon} - h(\varepsilon_{el})\dot{\varepsilon}$. It successfully helps in predicting foams mechanical properties (including storage and loss moduli G', G'').

The tensorial version of deformations in equation eq. (1) write $\bar{\bar{\varepsilon}}_{el}$, $\dot{\bar{\bar{\varepsilon}}}$ and $\dot{\bar{\bar{\varepsilon}}}_{pl}$. We have seen that they can be measured directly using the statistical deformations [1] $\bar{\bar{U}}$, $\bar{\bar{V}}$ and $\bar{\bar{P}}$, respectively. Here, we use these statistical notations for deformations, and eq. (1) becomes:

$$\frac{\mathcal{D}\bar{\bar{U}}}{\mathcal{D}t} = \bar{\bar{V}} - \bar{\bar{P}}\,. \tag{3}$$

Again, the elastic strain is loaded by the total applied deformation rate, that is, the velocity gradient; a process that is be limited by the plastic deformation rate.

A foam is a unique material where we can measure directly the velocity, deformation, and plastic rearrangements. We use tensorial statistical tools to extract the relevant information without useless details. We attempt at completely characterizing the T1s at large scale and describe the foam as a continuous medium. We want here to write an equation similar to eq. (2) valid in this tensorial case.

In the present manuscript, we suggest an analytical prediction of the rearrangements tensor : $\overline{\overline{P}}=\overline{\overline{P}}\left(\overline{\overline{U}},\overline{\overline{V}}\right)$, inspired by our scalar model [15]. Its orientation is determined from the foam's local elastic strain and its rate is determined from the foam's local total deformation rate. The relationship between experimental data agrees with our analytical prediction. Moreover, we correctly predict the spatial distribution of T1s, although it differs much from the spatial distribution of both deformation and elongation rate.

2 Model

2.1 Plasticity equation

The deviatoric elastic strain (shear, without dilation) is the traceless tensor

$$\overline{\overline{U}}_d \equiv \overline{\overline{U}} - \frac{1}{2}(\mathrm{Tr}\ \overline{\overline{U}})\ \overline{\overline{I}}\ . \tag{4}$$

Its amplitude is defined as

$$U_d \equiv \left[\frac{\overline{\overline{U}_d}:\overline{\overline{U}_d}}{2}\right]^{1/2}, \tag{5}$$

where we used the double contraction product of rank two tensors $\overline{\overline{A}}:\overline{\overline{B}}=\sum_{i,j} A_{ij}B_{ij}$. In a 2D configuration, U_d provides the absolute value of the eigenvalues of tensor $\overline{\overline{U}}_d$. The tensor $\overline{\overline{U}}_d\ /U_d$ is then a directionnal tensor that writes $diag(1,-1)$ in the eigenvector basis of elongation. For details of notations see [1].

We assume that if the applied deformation rate $\overline{\overline{V}}$ is in the direction opposed to internal strain ($\overline{\overline{V}}:\overline{\overline{U}}_d$ is negative), it contributes to unload it elastically. It thus does not induce many rearrangements [8]: we neglect them by setting $\overline{\overline{P}}$ to zero :

$$\text{if} \quad \overline{\overline{V}}:\overline{\overline{U}}_d<0, \qquad \overline{\overline{P}}=0. \tag{6}$$

In the opposite case, the applied deformation rate $\overline{\overline{V}}$ can induce T1s when it is in the same direction as the existing elastic strain: that is, if their scalar product $\overline{\overline{V}}:\overline{\overline{U}}_d$ is positive. In that case we postulate that the rearrangement tensor is:

$$\text{if} \quad \overline{\overline{V}}:\overline{\overline{U}}_d>0, \quad \overline{\overline{P}}=h(U_d)\frac{(\overline{\overline{V}}:\overline{\overline{U}}_d)\ \overline{\overline{U}}_d}{2{U_d}^2}. \tag{7}$$

The total deformation rate is "projected" onto the elastic strain tensor, which appears more clearly writing that the "norm" of the elastic strain is defined with $||\ \overline{\overline{U}}_d\ ||^2 = \overline{\overline{U}}_d:\overline{\overline{U}}_d = 2U_d^2$. If $\overline{\overline{V}}$ is proportional ("aligned") to $\overline{\overline{U}}_d$, it is then easy to show that Eq. (7) implies $\overline{\overline{P}}= h(U_d)\ \overline{\overline{V}}$. Moreover, if U_d has reached the yield value, $\overline{\overline{P}}=\overline{\overline{V}}$.

We have introduced the plasticity function h, which is a scalar fonction of the deformation amplitude. A smooth appearance of plasticity can be described by a continuous variation of the plastic function h [18] between the value 0 and 1. Eq. (7) is a mean field approximation, as will become apparent below (section 3.2.1).

For a perfect plastic material that yields when the elastic strain reaches the value U_Y, the plasticity function $h\,(U_d)$ discontinuously jumps from the value 0 when $U_d < U_Y$ and is 1 when $U_d \geq U_Y$, which we summarize with an Heaviside function:

$$h\,(U_d) = \mathcal{H}(U_d - U_Y) \tag{8}$$

The model is then the classical Prandtl-Reuss model for perfect plasticity [19]. The plastic evolution is directed along the preexistent elastic strain and occurs with a rate which is the projection of the total deformation rate onto the elastic strain.

2.2 Rearrangement frequency

When a rearrangement occurs, the total strain is not changed locally: the elastic strain decreases by $\delta\ \overline{\overline{\varepsilon}}_{el}= -\delta\ \overline{\overline{U}}$, and the plastic strain increases by $\delta\ \overline{\overline{\varepsilon}}_{pl}= \delta\ \overline{\overline{U}}$. This jump in deformation is distributed in space: it rapidly decays with the distance to the rearrangement location (see continuous model [9]). If, for simplicity, we consider that the deformation is uniformly concentrated over the area attributed to one link $A_{link} = A/N_{link}$, with a constant amplitude ϵ_0, we can write:

$$\delta\ \overline{\overline{U}}= \epsilon_0\ \frac{\overline{\overline{U}}_d}{U_d}, \tag{9}$$

where we assumed that rearrangements are aligned with elasticity (following eq. 7). The plasticity rate tensor $\overline{\overline{P}}= \delta\ \overline{\overline{\varepsilon}}_{pl}\ /\delta t$ thus writes:

$$\overline{\overline{P}}= f\ \delta\ \overline{\overline{U}}, \tag{10}$$

where f is the frequency of rearrangements *per link* ($f = \dot{n}_a = \dot{n}_d$). When considering averages in larger counting boxes, containing N_{link} links (approximately 3 times the number of bubbles in the box), equation (10) still holds and writes $\overline{\overline{P}}= f_{box}\ \delta\ \overline{\overline{U}}_{box}$. Indeed the frequency in the counting box is $f_{box} = N_{link} f$, and the impact of a T1 on a larger surface is diluted to the value $\delta\ \overline{\overline{U}}_{box}= \delta\ \overline{\overline{U}}\ /N_{link}$.

Combining the plasticity equation (eq. 7) and the amplitude of stress relaxation (eq. 9), we obtain the frequency

f of T1 events, per link:

$$\text{if} \quad \overline{\overline{V}} : \overline{\overline{U}}_d > 0, \quad f = \frac{h(U_d)}{2\epsilon_0 U_d} \left(\overline{\overline{V}} : \overline{\overline{U}}_d \right),$$
$$\text{if} \quad \overline{\overline{V}} : \overline{\overline{U}}_d < 0, \quad f = 0. \qquad (11)$$

It depends on the positive eigenvalue $\dot{\varepsilon}$ of the elongation rate, and on the relative angle θ between the eigenvectors of the elongation rate and deformation:

$$\text{if} \quad \cos(2\theta) > 0, \quad f \propto \cos(2\theta)\dot{\varepsilon}.$$

This extends findings by [17]. It expresses that rearrangements are frequent where the total deformation rate is strong, and when the elongation rate is parallel to the pre-existing strain thus loading it through the yield surface.

At the yield point, $h = 1$, the frequency is such that the loading rate of the norm of strain $dU_d/dt = \overline{\overline{U}}_d : (d\,\overline{\overline{U}}_d/dt)/2U_d$ is exactly balanced by the topological relaxation rate $f\delta(U_d) = f\ \overline{\overline{U}}_d : \delta\,\overline{\overline{U}}\ /2U_d$ according to eq. (9).

3 Experimental tests

The prediction (eq. 7) uses a tensorial formalism, so that it equally applies to 2D or 3D systems. For simplicity, we test it in on bubble monolayers (quasi-2D foams) which flow horizontally (true 2D velocity field). A large set of detailed data is available; bubbles act as convenient tracers of elastic strain, rearrangements and velocity [5,20,21,22,1].

3.1 Materials and methods

We reanalyse data already published and courteously provided to us by the authors. For details of the materials and methods, see the original publications.

In Figs. (1a-c), the channel (only partly visible) is horizontal, its length is 1 m, its width 10 cm, its thickness 3.5 mm. It is filled with bubbles obtained by steadily blowing nitrogen in water with 1% commercial dishwashing liquid. Coalescence and ageing are below detection level. The bubbles are monodisperse (area $A_{bubble} = 16.0$ mm^2, fluid fraction $\approx 7 \pm 1\%$) and form a disordered monolayer which reaches the free exit at the end of the channel. The resulting steady plug flow, well in the quasistatic regime [4], is made hetereogeneous by inserting a 3 cm diameter obstacle (Fig. 1a,b) or a constriction [5] (Fig. 1c). Thus different regions simultaneously display different velocity gradients, elastic strains, and rearrangement rates, and allow to sample simultaneously many different conditions.

In Fig. (1a), the foam is confined between the surface of water and a horizontal plate of glass. Bubbles are rather round, due to the high effective liquid fraction [7]. Thus the region where T1s occur is larger, more widely distributed around the obstacle (compare Figs. (8) and (10) below). There are thus more regions of the flow where statistics are significant. This is why we use this experiment for the most detailed quantitative tests (section 3.2).

In Fig. (1d) the foam is in a 2D circular Couette geometry [6]. Briefly, the foam is confined vertically between two parallel glass plates, 2 mm apart; and horizontally between two concentric disks (only partly visible) with semicircular teeth of radius 1.2 mm to match the bubble diameter, thus anchoring bubbles at the walls. The outer disk, of radius 122 mm, is fixed. The inner disk, of radius 71 mm, rotates at 0.25 mm s^{-1}, thus shearing the foam. The resulting velocity field decreases quickly with the distance to the inner disk. This experiment has stirred a debate about the existence and cause of velocity localisation: for review, see for instance ref. [23]. The experimental measurements we present here complement those of ref. [20]; they are largely model-independent and might be used in the future to contribute to this debate.

We estimate the amplitude of deviatoric part $\overline{\overline{P}}_d$ of plastic deformation with the amplitude $P_d = (\overline{\overline{P}}_d : \overline{\overline{P}}_d\ /2)^{1/2}$, and the amplitude of the deviatoric part of the total deformation rate with $V_d = (\overline{\overline{V}}_d : \overline{\overline{V}}_d\ /2)^{1/2}$. In these experiments $\overline{\overline{P}}$ and $\overline{\overline{V}}$ are nearly parallel, so that the prediction of equation (7) can be projected on the same axis: we obtain a direct measurement of the plasticity fraction as $h \simeq P_d/V_d$. Knowing the shape of the plasticity fraction, we obtain from eq. (7) a prediction regarding the position, frequency, orientation and anisotropy of rearrangements. We plot it as a map to facilitate the comparison with actual measurements.

3.2 Graphs

This section uses data of Fig. (1a).

3.2.1 Rearrangements: orientation and frequency

Fig. (4) seems to confirm the mean field approximation of the model (eq. 7), namely that disappearing and appearing links are determined (in average) by the existing strain. More precisely, $\overline{\overline{P}}$ makes an angle of $0 \pm 9°$ with $\overline{\overline{M}}$ or $\overline{\overline{U}}$: disappearing links ℓ_d are mainly in the elongation direction (Fig. 4, top). Their length is 1.2±0.1 times larger than the average of existing links in that direction, $\ell_+ = \sqrt{2\lambda_1}$, where λ_1 is $\overline{\overline{M}}$'s largest eigenvalue (Fig. 4, middle). Conversely, links ℓ_a appear in the contracted direction of $\overline{\overline{M}}$, with a length 1.1±0.1 times the average of existing links, $\ell_- = \sqrt{2\lambda_2}$ (Fig. 4, bottom).

The jump in elastic strain is therefore oriented with $\overline{\overline{U}}$. Its amplitude is approximately:

$$\delta\,\overline{\overline{U}} \approx \begin{pmatrix} \frac{\ell_d^2}{\ell_+^2} & 0 \\ 0 & \frac{-\ell_a^2}{\ell_-^2} \end{pmatrix} \approx \begin{pmatrix} 1.3 \pm 0.2 & 0 \\ 0 & -1.2 \pm 0.2 \end{pmatrix}, \qquad (12)$$

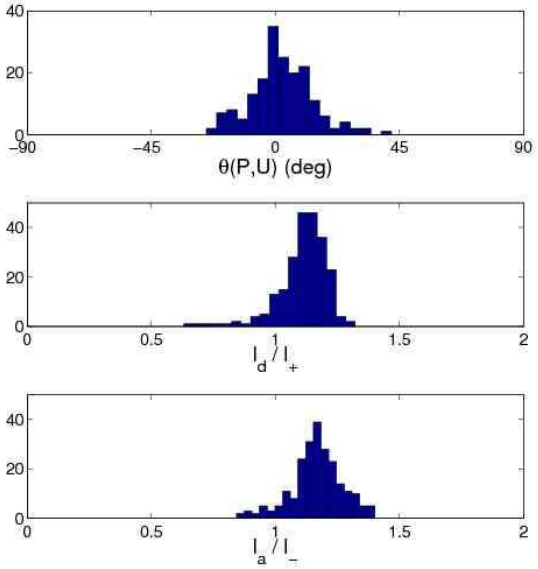

Fig. 4. Histograms of measurements in all regions of the foam (Fig. 1a). Top: angle between topological events and elongation. Middle: length of disappearing links compared to average length in elongation direction ℓ_+. Bottom: length of appearing links compared to average length in compressed direction ℓ_-.

using $\delta \bar{\bar{U}} \approx \delta \bar{\bar{M}} \times \bar{\bar{M}}^{-1}/2$, from the differentiation of the definition of the tensor $\bar{\bar{U}}$. We conclude from equation (9) that each rearrangement changes the elastic strain per link by a constant amount:

$$\epsilon_0 \simeq 1.2 \pm 0.2. \tag{13}$$

Strain is decreased by slightly more than one average length in the elongation direction, and increased by slightly more than one average length in the orthogonal direction.

Rearrangement frequency is well predicted (Fig. 5) by equation (11). The main parameter required, namely U_Y, is directly read from measurements of U: here $U_Y = 0.15$, which is reasonable for a foam with 4% liquid fraction. Second, the shape of the elasto-plastic transition has been chosen as a quadratic h function, which is justified further.

3.2.2 Transient rheometry along a streamline

The origin of the upstream/downstream asymmetry of plasticity can now be qualitatively explained, by following a bubble along its streamline (Fig. 6). The obstacle imposes a succession of symmetric opposite elongation rates: spanwise before the obstacle, and streamwise after it (Fig. 8). Before the obstacle, the elastic strain and the elongation rate are aligned, and the foam is yielding. After the obstacle, it takes some time until the bubbles fully relax, then deform again in the new direction of elongation, orthogonal to the initial one (Fig. 7). Topological rearrangements are therefore concentrated in a smaller region. Because of the elastic nature of the foam, the plastic flow depends on the elongation rate and on the present amplitude of elastic strain.

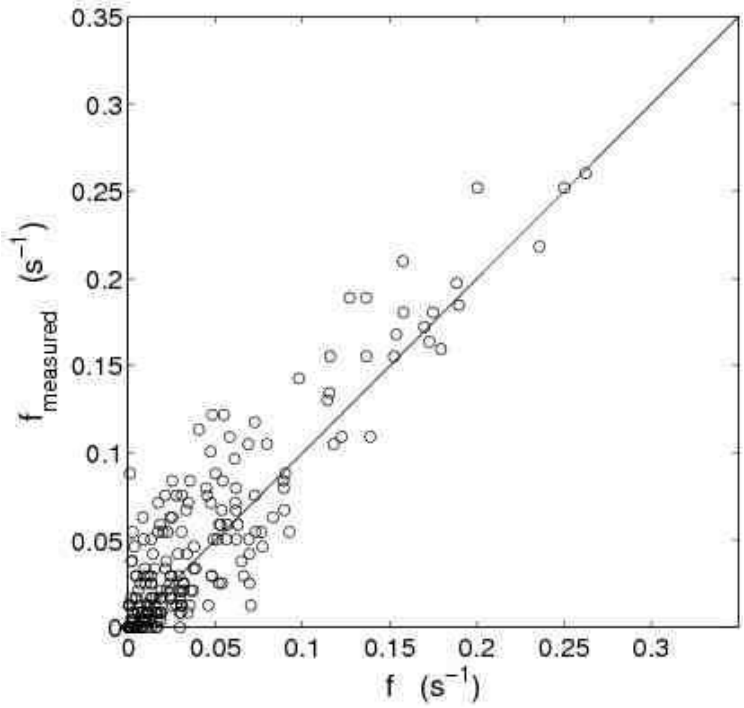

Fig. 5. Frequency of rearrangements: observed *versus* predicted. Each point corresponds to one region of the foam, that is, one ellipse of Fig. (8). Observations: frequency f_{measured} of rearrangements (per link and second) mesured on Fig. (1a). Predictions: f from eq. (11), setting the yield function to $h = \min((U/U_Y)^2, 1)$ and the yield $U_Y = 0.15$, while $\epsilon_0 = 1.2$ (eq. 13). Solid line: diagonal $f_{\text{measured}} = f$.

3.3 Maps

This section presents the spatial distribution of measurements plotted as ellipse maps (tensor fields), which simultaneously display: position, orientation, anisotropy and frequency of rearrangements. Again, we predict plasticity from the measured elastic strain and total strain rate, using a yield deformation U_Y directly read from measurements of U, without adjustable parameter. A smooth quadratic plasticity fraction h is chosed (as observed from rheometric measurements [15]), to account for possible plastic events below the yield.

3.3.1 Flow around an obstacle: wet foam

For a wet foam, upon flowing around the obstacle (Fig. 1a), we observe that the amplitude of $\bar{\bar{U}}$ increases then decreases, while $\bar{\bar{V}}$ changes orientation.

The agreement between prediction and measurement of $\bar{\bar{P}}$ is very good (Fig. 8). In particular, we predict well the spatial distribution of T1 events: they occur mostly just before the obstacle, and in a narrower region after it. For horizontal positions just on the right of the center of the obstacle, the flow tends to decrease the existing strain ($\bar{\bar{V}}$:$\bar{\bar{U}}_d < 0$): the predicted frequency vanishes.

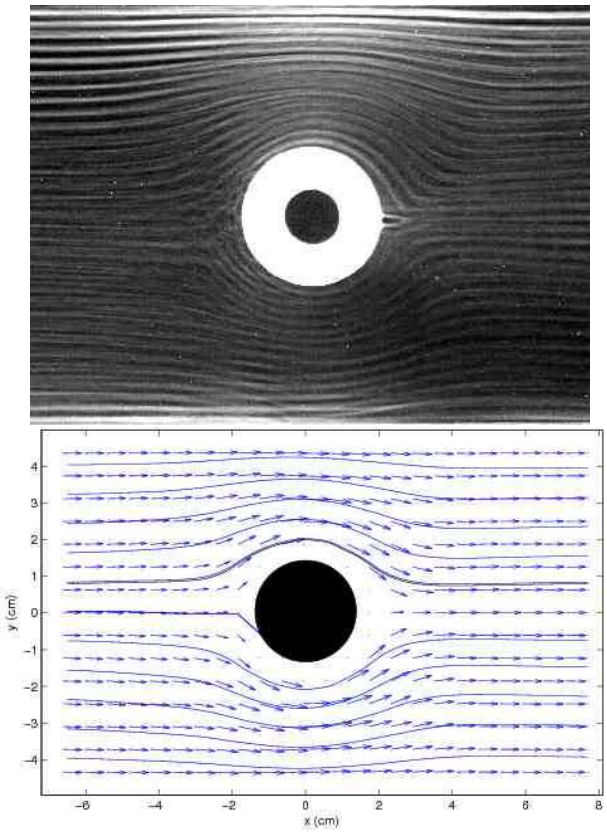

Fig. 6. Foam flow. Top: superimposed images evidence the streamlines (here from Fig. (1b)). Bottom: measured velocity field and streamlines. The solid line highlights the streamline analysed in Fig. (7).

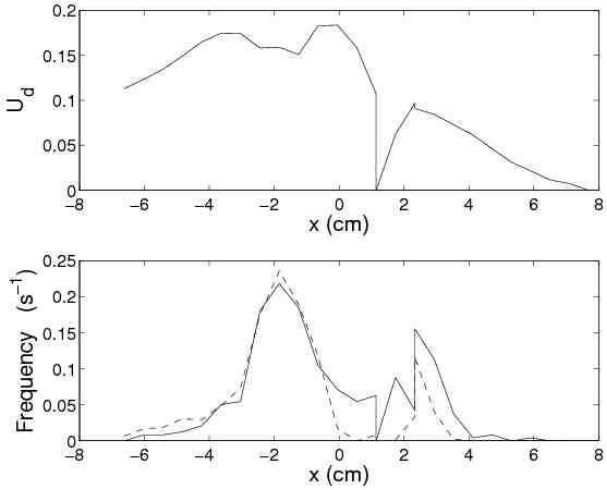

Fig. 7. Measurements along the streamline shown on Fig. (6)bottom. Top: loading and unloading of elasticity, U_d. Bottom: T1 frequency along streamline, as in Fig. (5); solid line: experimental f_{measured}; dashes, predicted f.

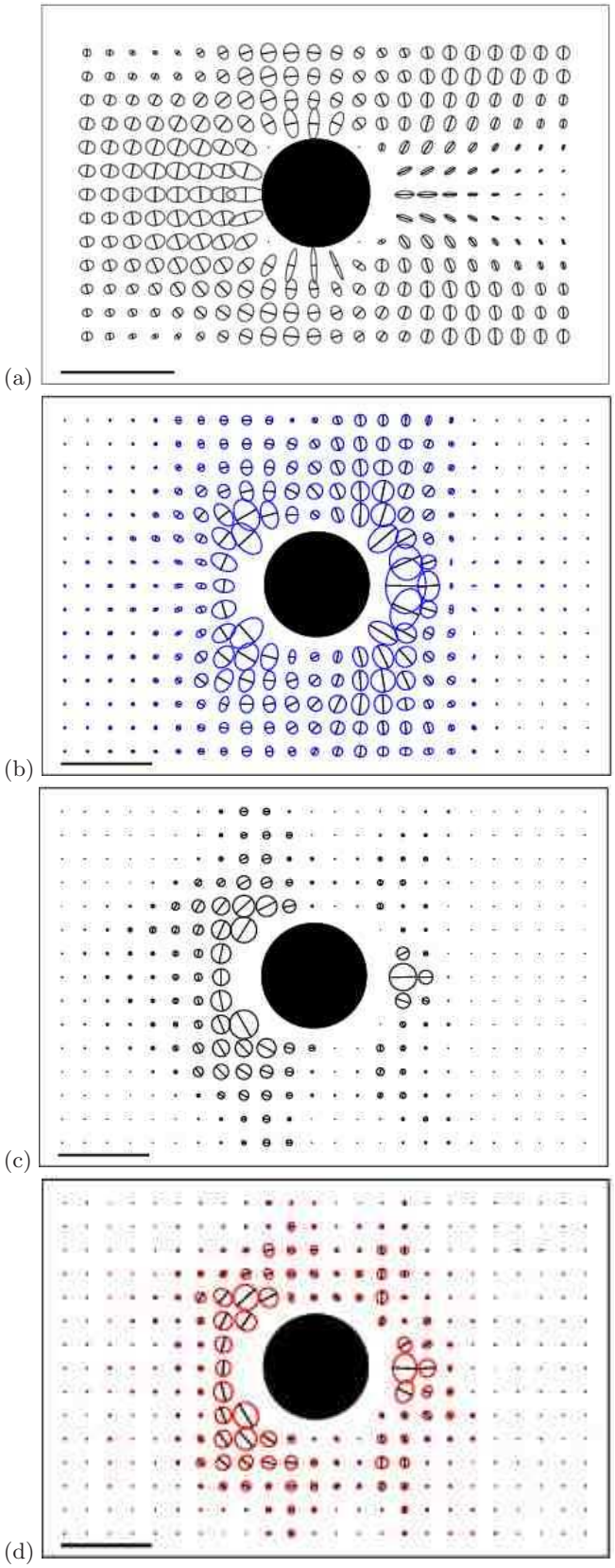

Fig. 8. Wet foam flowing around an obstacle (Fig. 1a). Measurements of $\overline{\overline{U}}$ (a) and $\overline{\overline{V}}$ (b) yield, through eq. (7) with quadratic plasticity function h, the theoretical prediction of $\overline{\overline{P}}$ (c), in good agreement with its measurement (d). Scale: for $\overline{\overline{U}}$, bar= 1 (no unit); for $\overline{\overline{V}}$ and $\overline{\overline{P}}$: bar= 1 s^{-1}.

We also predict well the direction of rearrangements, as well as their amplitude, represented by the direction of the coffee beans and their size, respectively. We do not observe in experiment purely elastic areas and purely plastic areas with a sharp transition line, which justify the use of non vanishing h function below the yield for the prediction.

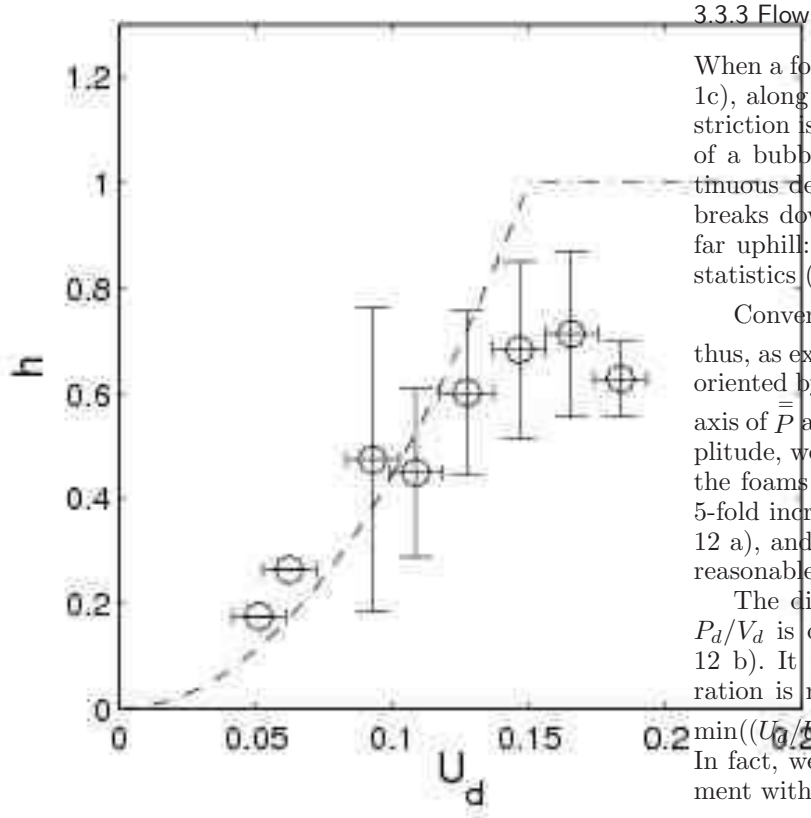

Fig. 9. Estimate of h. Symbols: measurements from Fig. (1a) of $P_d/V_d \simeq h$. We represented the average (circle) and standard deviation (vertical error bar) after binning data along the horizontal axis on equal interval sizes (horizontal error bar). Dash-dots: interpolation $h(U_d) = \min((U_d/U_Y)^2, 1)$, quadratic up to $U_Y = 0.15$.

Conversely, statistics are just good enough that we can extract h from measurements. (Fig. 9). We observe that h increases, more or less like the proposed $(U/U_Y)^2$, up to $U_Y = 0.15$, then saturates. Interestingly, it plateaus at a value $\sim 0.6 \pm 0.1$ significantly lower than 1. This is probably because after the obstacle $\overline{\overline{V}}$ unloads $\overline{\overline{U}}$, which decreases before the foam enters the fully plastic regime.

3.3.2 Flow around an obstacle: dry foam

The same experiment with a dry foam (Fig. 1b) yields a qualitatively similar behaviour for $\overline{\overline{U}}$, $\overline{\overline{V}}$ and $\overline{\overline{P}}$ (Fig. 10). Quantitatively, however, the maximum value of U_d is here 0.45, which is a reasonable value for a dry foam [14]. The spatial variation of $\overline{\overline{U}}$, $\overline{\overline{V}}$ and $\overline{\overline{P}}$ is restricted to a much narrower range.

This means that we measure larger values but on much less points, resulting in poorer statistics. Still, the agreement between prediction and measurements of $\overline{\overline{P}}$ is qualitatively correct. Extracting h from the data is also qualitative, with apparently a plateau as low as 0.4 (Fig. 11).

3.3.3 Flow through a constriction.

When a foam is forced to flow through a constriction (Fig. 1c), along any streamline U_d steadily increases. The constriction is here so narrow, comparable to the square root of a bubble area, that just at the constriction the continuous description (and thus our measurement method) breaks down. The influence of the constriction is visible far uphill: U_d is widely distributed, and we obtain good statistics (Fig. 13).

Conversely, $\overline{\overline{V}}$ is more localised near the orifice, and thus, as expected from eq. (7), so is $\overline{\overline{P}}$. Plasticity is indeed oriented by the elastic strain, the angle between the main axis of $\overline{\overline{P}}$ and of $\overline{\overline{U}}_d$ is $1 \pm 5°$. Concerning the plasticity amplitude, we observe that P_d is much smaller than V_d when the foams enters in the field of view: P_d/V_d undergoes a 5-fold increase until it reaches 1 at the constriction (Fig. 12 a), and U_d plateaus. We measure $U_Y \sim 0.32$; which is reasonable for a foam with $\sim$1% liquid fraction..

The direct estimate of the plasticity fraction as $h \simeq P_d/V_d$ is obtained with reasonably good statistics (Fig. 12 b). It plateaus close to 1, confirming that the saturation is reached. We thus inject the function $h(U_d) = \min((U_d/U_Y)^2, 1)$ in eq. (7) to improve the prediction of $\overline{\overline{P}}$. In fact, we obtain an extremely good quantitative agreement with the measurement (Fig. 13).

3.3.4 Couette flow

In a steady Couette flow (Fig. 14), as expected $\overline{\overline{U}}$ respects the circular symmetry: it does not vary orthoradially. The advantage is that we can improve the measurements by averaging orthoradially. The drawback is that we have very few independent measurements (here 6), along the radial direction. $\overline{\overline{U}}$ is significantly different from zero eveywhere. Near the rotating (inner) disk, it means that $\overline{\overline{U}}$ saturates. Near the fixed (outer) disk, it is probably a residual strain due to the foam preparation (there are not enough T1s to relax it). U_d is rather low (at most of order of 0.1), which is consistent with the high liquid fraction. All these findings confirm those of ref. [20].

As expected, $\overline{\overline{V}}$ similarly does not vary orthoradially. It decreases quickly with the distance to the fixed disk, so that we have only two independent, non-zero measurements. It is thus impossible to perform the same analysis as in the above flows which truly vary with both space coordinates.

Still, we can predict $\overline{\overline{P}}$ from eq. (7): this agrees quantitatively with the measurements. Concerning the orientation of $\overline{\overline{P}}$, the angle between the main axis of $\overline{\overline{P}}$ and of $\overline{\overline{U}}$ is

$-5 \pm 3°$, they are indeed aligned. Since the flow is steady, $\overline{\overline{U}}$ is constant along streamline, and we thus expect $\overline{\overline{P}}$=$\overline{\overline{V}}$: this agrees only qualitatively with the measurements.

4 Conclusion

Using the formalism developed in the companion paper [1], we measure in different 2D foam flows the tensors which quantify the elastic strain, the total deformation rate and the plastic rearrangements. We then generalise to tensors a previous scalar model [15], and base it on local measurements on individual bubbles.

We show that the plastic rearrangements arise from a combination of both the elastic strain and the total deformation rate. As shown by the maps, they cannot be predicted from the elastic strain alone, nor from the total deformation rate alone.

For instance, in the wet obstacle flow, the spatial symmetry with respect to the obstacle is very different in the three maps. In the dry foam obstacle, the elastic strain extends very far, while the velocity gradient has a narrower extension, but both are needed, and the total deformation gives the orientation. In the constriction the elastic strain extends so much that it is mainly the total deformation rate which determines where T1s occur.

In a first approximation, the plasticity is described mainly by the behaviour near yielding. The yield deformation U_Y is the main relevant parameter. We determine it directly from image analysis and check that the obtained values are reasonable. We then statistically predicts the position, orientation, anisotropy and frequency of topological rearrangements in a flowing foams, in good agreement with various experiments.

In a second step, to refine the description and improve the prediction, we introduce the proportion of plasticity, to account for the gradual appearance of plasticity instead of a sharp yield. It is a function $h(U_d)$ (also called "yield function") of the elastic strain, which interpolates between 0 (fully elastic) at small deformation $h(0) \sim 0$, and 1 (fully plastic) near yielding, $h(U_Y) \sim 1$. We obtain here estimates of h.

A third, even more refined step (not studied here) might involve not only the average values of the tensors, but also their spatial and temporal fluctuations. This three-step approach is similar to that in the scalar case [15].

5 Perspectives

The prediction of plastic rearrangements is a necessary step to close the system of equations describing the foam dynamics. The fact that our measured fields vary smoothly with space make us confident that we can obtain a continuous description of 2D foam flows. That is, partial differential equations should be able to predict, just from the boundary conditions, all tensors: including the elastic strain and the total deformation rate, which are here measured but not predicted. The missing equation is a dynamical equation that would relate stresses to strains. The scalar model [15] was proposing a total stress that is the sum of the elastic and viscous stress: $\sigma = \mu\varepsilon_{el} + \eta\dot{\varepsilon}$, with μ an elastic modulus and with η a viscosity. A tensorial generalisation is

$$\overline{\overline{\sigma}} = 2\mu\, \overline{\overline{U}}_d + K\, \mathrm{Tr}(\overline{\overline{U}}) + 2\eta\, \overline{\overline{V}}, \qquad (14)$$

with the addition of a compression modulus K, which is in practice much larger than the shear modulus for foams. This equation, in addition to the kinematic equation for elastic strain proposed in the present article (Eqs. 3 and 7), provides a fully closed constitutive equation for foam materials. Further work will be needed to obtain complete predictions and compare them with experiments. This is already possible for a flow which depends on one space coordinate, like the 2D Couette flow of (Fig. 1d) [24]. The prediction of the other flows presented (Fig. 1a-c) here is in progress.

It appears necessary and sufficient to determine h for various foams. While here we have first indirect estimates, a catalogue of h measured directly, for foams with different liquid fractions and disorders, is in progress.

Nothing prevents our predictions from being extended to 3D, and detailed measurements are in progress. Extension to higher shear rates [10] is challenging, but not impossible in principle. While some of our results are specific to foams, the general approach which links individual and collective behaviours might be applicable to other complex materials.

Acknowledgments

We warmly thank B. Dollet, M. Asipauskas, and G. Debrégeas for kindly providing published and unpublished raw data.

References

1. F. Graner, B. Dollet, C. Raufaste, P. Marmottant, preprint
2. D. Weaire, S. Hutzler, *The physics of foams* (Oxford University Press, Oxford, 1999)
3. A. Saint-Jalmes, D. Durian, J. Rheol. **43**, 6 (1999)
4. B. Dollet, F. Elias, C. Quilliet, C. Raufaste, M. Aubouy, F. Graner, Phys. Rev. E **71**, 031403 (2005)
5. M. Asipauskas, M. Aubouy, J.A. Glazier, F. Graner, Y. Jiang, Granular Matt. **5**, 71 (2003)
6. G. Debrégeas, H. Tabuteau, J.M. di Meglio, Phys. Rev. Lett. **87**(17), 178305 (2001)
7. C. Raufaste, B. Dollet, S. Cox, Y. Jiang, F. Graner, to appear in Eur. Phys. J. E (2007)
8. C. Raufaste, unpublished (2007)
9. G. Picard, A. Ajdari, F. Lequeux, L. Bocquet, Eur. Phys. J. E **15**(371–381) (2004)
10. P. Saramito, Journal of Non-Newtonian Fluid Mechanics **In Press** (2007)
11. W.L. Bragg, J.F. Nye, Proc. R. Soc. London Ser. A **120**, 474 (1947)

12. A. Gouldstone, K.J. Van Vliet, S. Suresh, Nature **411**(6838), 656 (2001), ISSN 0028-0836
13. DoITPoMS, Dissemination of Information Technology for the Promotion of Materials Science, University of Cambridge, UK., `http://www.doitpoms.ac.uk/tlplib/dislocations`
14. H.M. Princen, J. Coll. Interf. Sci. **91**(1), 160 (1983)
15. P. Marmottant, F. Graner, accepted for Eur. Phys. J. E (2007)
16. A. Kabla, G. Debrégeas, Phys. Rev. Lett. **90**(25), 258303 (2003)
17. S. Vincent-Bonnieu, R. Höhler, S. Cohen-Addad, preprint
18. P. Marmottant, F. Graner, arxiv: cond-mat/0610261
19. K. Washizu, *Variational methods in elasticity and plasticity* (Pergamon Press, 1975)
20. E. Janiaud, F. Graner, J. Fluid Mech. **532**, 243 (2005)
21. B. Dollet, M. Aubouy, F. Graner, Phys. Rev. Lett. **95**, 168303 (2005)
22. B. Dollet, F. Graner, J. Fluid Mech. **585**, 181 (2007)
23. E. Janiaud, D. Weaire, S. Hutzler, Phys. Rev. Lett. **97**, 038302 (2006)
24. I. Cheddadi, C. Raufaste, P. Saramito, P. Marmottant, F. Graner, in preparation

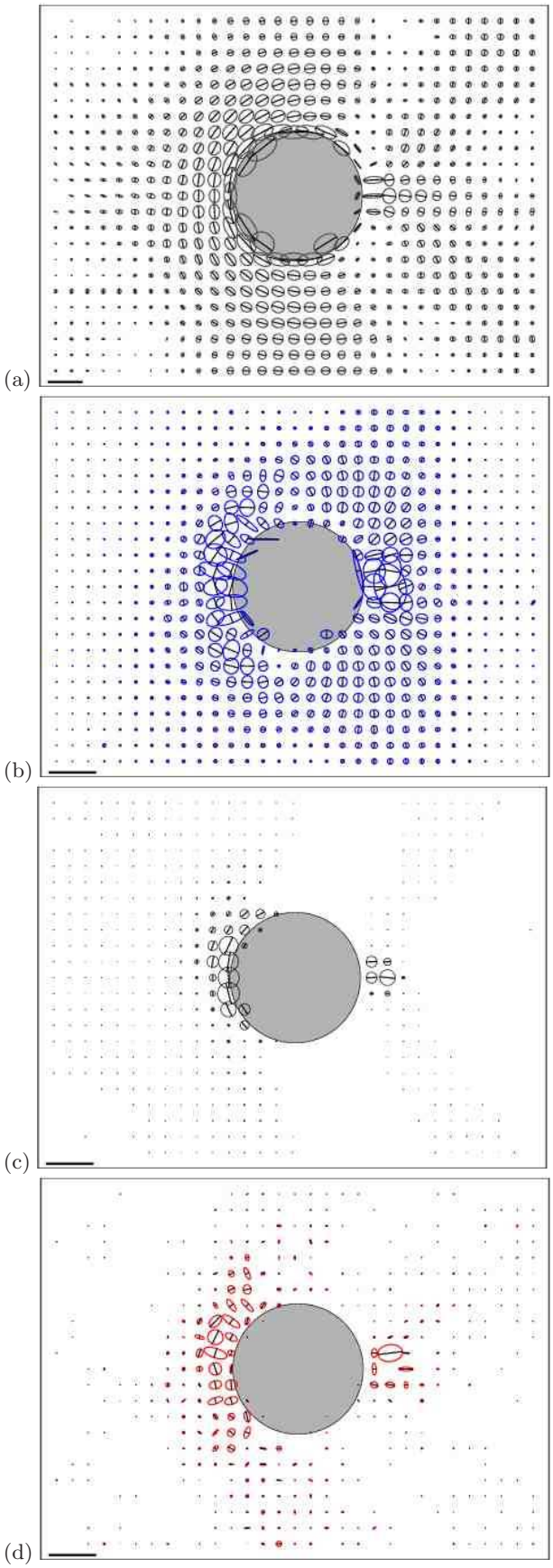

Fig. 10. Dry foam flowing around an obstacle (Fig. 1b). Same caption as Fig. (8), except that for $\overline{\overline{V}}$ and $\overline{\overline{P}}$ bar= 10 s^{-1}. See similar figures in the companion paper [1].

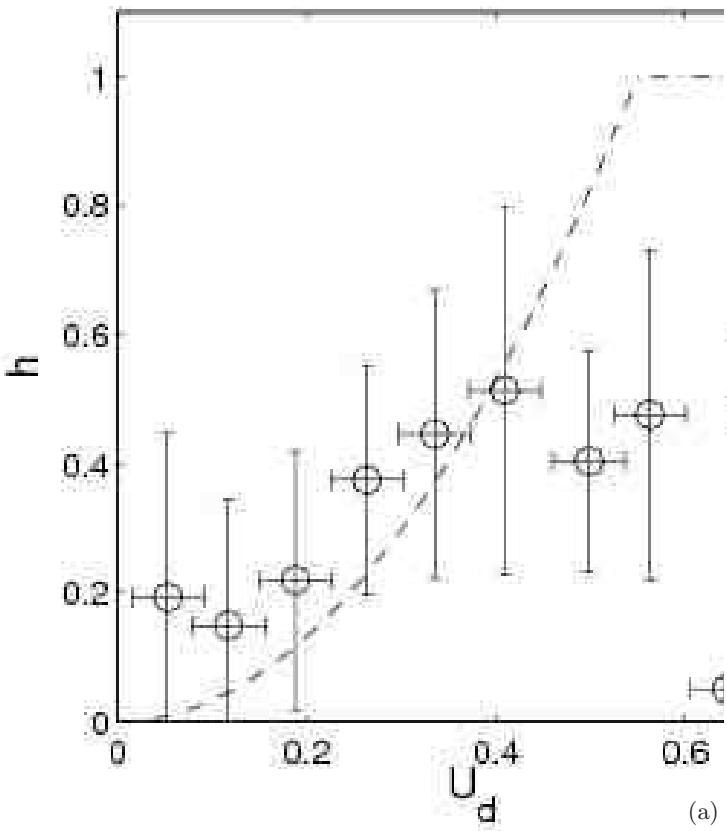

Fig. 11. Same figure as Fig. (9), but for the dry foam of Fig. (1b), $U_Y = 0.45$.

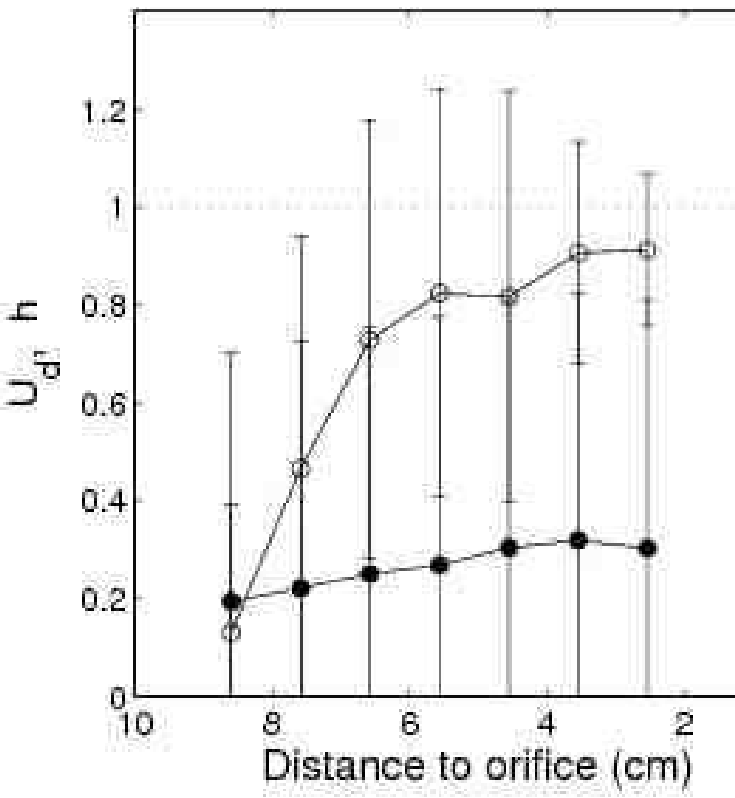

(a)

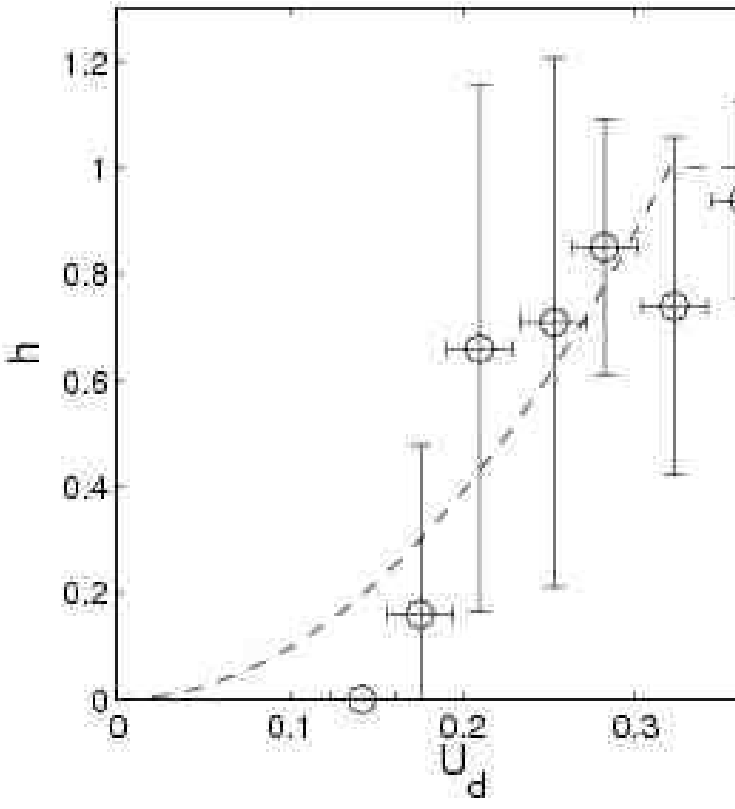

(b)

Fig. 12. Constriction: analysis of Fig. (1c). (a) P_d/V_d (open circles) and U_d (closed circles) *versus* the distance to the constriction. (b) Plasticity fraction h estimated as $h \simeq P_d/V_d$ *versus* strain U_d (data from (a)): same figure as Figs. (9) and (11), here with $U_Y = 0.32$.

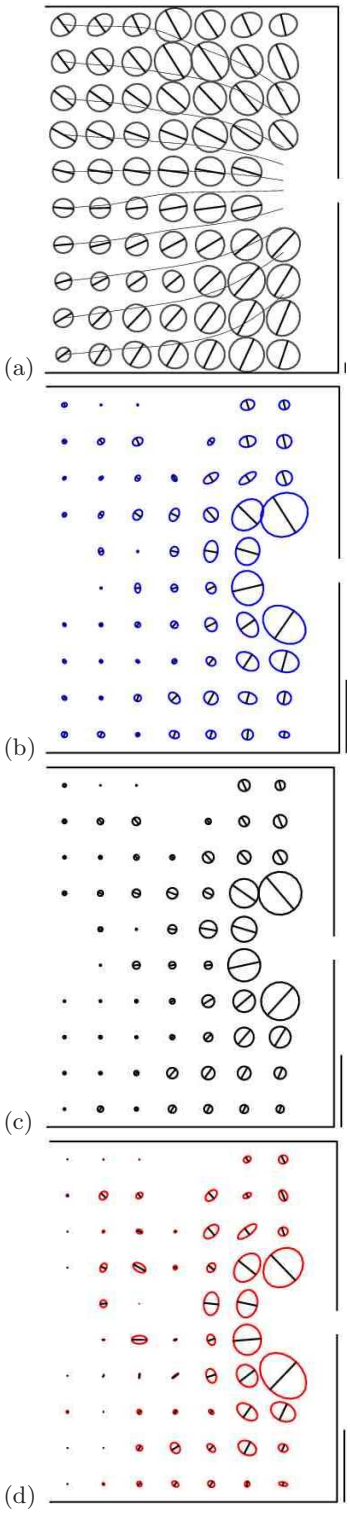

Fig. 13. Foam flowing through a constriction (Fig. 1c). Same caption as Fig. (8), except that for $\overline{\overline{U}}$ bar$= 0.1$, and for $\overline{\overline{V}}$ and $\overline{\overline{P}}$ bar$= 0.01$ s^{-1}. See similar figures in the companion paper [1].

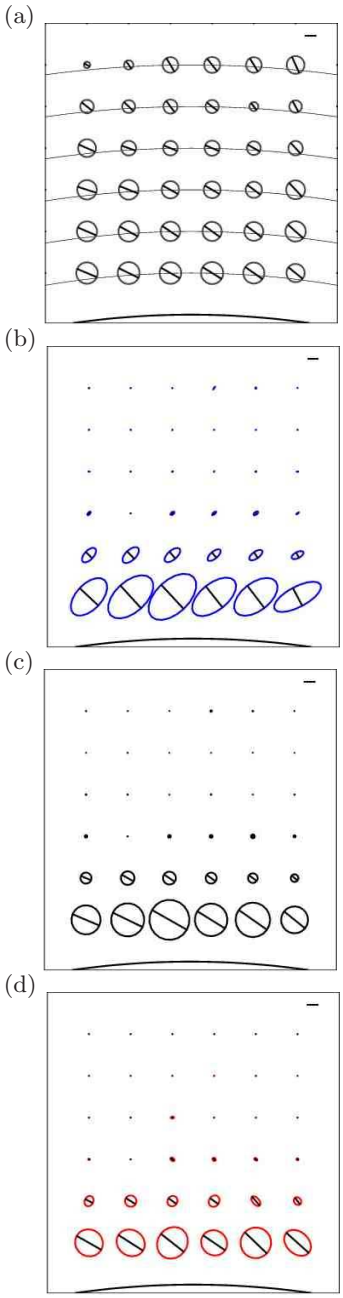

Fig. 14. Foam sheared between concentric disks (Fig. 1d). Same caption as Fig. (8), except that for $\overline{\overline{U}}$ bar$= 0.1$, and for $\overline{\overline{V}}$ and $\overline{\overline{P}}$ bar$= 0.01$ s^{-1}.